JYX JYVÄSKYLÄN YLIOPISTO UNIVERSITY OF JYVÄSKYLÄ

This is a self-archived version of an original article. This version may differ from the original in pagination and typographic details.

Author(s): Malkiewicz, T.; Lhersonneau, G.; Fadil, M.; Jacobsson, U.; Jones, P.; Helariutta, K.; Karvonen, P.; Khlebnikov, S.; Trzaska, W. H.

Title: Production of a 15C radioactive ion beam based on 18O(n, α)

Year: 2019

Version: Published version

Copyright: © The Author(s) 2019.

Rights: CC BY 4.0

Rights url: https://creativecommons.org/licenses/by/4.0/

Please cite the original version:

Malkiewicz, T., Lhersonneau, G., Fadil, M., Jacobsson, U., Jones, P., Helariutta, K., Karvonen, P., Khlebnikov, S., & Trzaska, W. H. (2019). Production of a 15C radioactive ion beam based on 18O(n, α). European Physical Journal A, 55(6), Article 88. https://doi.org/10.1140/epja/i2019-12761-y

Eur. Phys. J. A (2019) **55**: 88
DOI 10.1140/epja/i2019-12761-y

THE EUROPEAN PHYSICAL JOURNAL A

Regular Article – Experimental Physics

Production of a ^{15}C radioactive ion beam based on ^{18}O(n, α)

T. Malkiewicz[1,a], G. Lhersonneau[2], M. Fadil[3], U. Jacobsson[4], P. Jones[5], K. Helariutta[4], P. Karvonen[6], S. Khlebnikov[7], and W.H. Trzaska[8,b]

[1] CSC-IT Center for Science Ltd., P.O.Box 405, Keilaranta 14, 02101 Espoo, Finland
[2] 189 Allée Jules Verne, 075000 Guilherand-Granges, France
[3] GANIL, Bld Henri Becquerel, B.P. 55027, 14076 Caen Cedex 05, France
[4] Department of Chemistry, University of Helsinki, P.O.Box 55, 00014 Helsinki, Finland
[5] iThemba Laboratory for Accelerator Based Science, P.O.Box 722, Somerset West 7129, Western Cape, South Africa
[6] Power Division, Fortum Corporation, P.O.Box 100, Keilaniementie 1, 02101 Espoo, Finland
[7] Khlopin Radium Institute, 2 Murinsky Av. 28, Saint Petersburg, Russia
[8] Department of Physics, University of Jyvaskyla, P.O.Box 35, 40351 Jyvaskyla, Finland

Received: 22 January 2019 / Revised: 10 April 2019
Published online: 7 June 2019
© The Author(s) 2019. This article is published with open access at Springerlink.com
Communicated by P. Woods

Abstract. In the context of the SPIRAL2 radioactive beam facility the production rate of the neutron-rich ^{15}C nucleus by ^{18}O(n, α) has been investigated. In a water target of 20 cm^3, enriched in ^{18}O and placed behind the neutron converter, a rate of a few 10^{10} nuclei per second can be reached with 1 mA of 40 MeV deuterons. A ^{18}O(n, α) cross-section based on the activation method is proposed. It is intermediate between the highest and lowest evaluations available to date.

Introduction

The SPIRAL2 project at GANIL, Caen, France, is designed to extend the range of nuclear physics experiments, especially to neutron-rich and very heavy nuclei [1,2]. The first stage of SPIRAL2 is a high-intensity linear driver able to produce, among other applications, beams of energetic neutrons by stopping deuteron beams in the so-called converter target. The Neutrons-for-Science (NFS) program for neutron experiments [3] is starting.

The most ambitious project is certainly the production of beams of neutron-rich fission products, based on fission of natural uranium with fast neutrons. As a complement, production schemes of nuclei lighter than fission products have been evaluated. That study has been carried out in the frame of the FP7 program of the European Commission and resulted in a PhD [4]. One of the nuclei investigated as a candidate for a post-accelerated beam has been ^{15}C. The only suitable reaction seemed to be ^{18}O(n, α)^{15}C. Neutron production with a deuteron beam of 40 MeV has been measured [5]. The flux of neutrons above 4 MeV is about 0.7% per deuteron in a target close enough to intercept neutrons emitted up to 30 degrees from the beam axis. This converts to $4.3 \cdot 10^{13}$ neutrons/s for a 1 mA deuteron current. However, technical aspects of the envisaged ISOL-based concept were not encouraging. The natural abundance of ^{18}O of only 0.2% requires a high degree of enrichment. The cost is hardly compatible with a high-temperature solid oxyde target which necessarily deteriorates and needs to be replaced. In addition, efficient release of ^{15}C ($t_{1/2} = 2.45$ s) from such a target is *a priori* problematic. These considerations let the ^{15}C beam project to be, at least, postponed.

An alternative appeared yet during informal discussions among some of the authors of this work. Water enriched in ^{18}O is commercially available. One major use of it is to be bombarded by protons to generate the ^{18}F positron source for Proton-Electron-Tomography, *e.g.* ref. [6] that is used *e.g.* for clinical imaging of cancer and of some neurological diseases. A water target at room temperature should be suitable for extracting carbon. The native ^{15}C would combine with oxygen in suspension and quickly leave the liquid as CO_2 bubbles.

When a possible solution to two major technical challenges was found, it became interesting to test the production of ^{15}C experimentally. There apparently do not exist experimental cross-section data, though the National Nuclear Data Center [7] lists evaluations based on models in the ENDF data library. The cross-sections shown for ^{18}O(n, α)^{15}C span a wide range in amplitude. A single measurement of production rate of ^{15}C with a 40 MeV deuteron beam was the primary goal of this work. Yet,

[a] e-mail: tomasz.malkiewicz@csc.fi
[b] e-mail: wladyslaw.h.trzaska@jyu.fi (corresponding author)

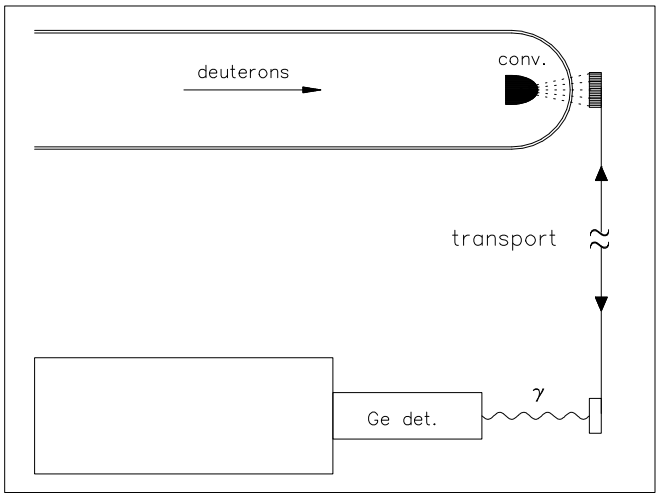

Fig. 1. Schematic layout of the experiment, not on scale. The neutrons generated in the converter target activate either the foils used to measure the neutron spectrum or react with ^{18}O in the water target to produce ^{15}C. For a detailed description, see ref. [9].

there was an opportunity to obtain a rough estimate of the ^{18}O(n, α)^{15}C cross-section by measuring the energy distribution and flux of the neutrons impinging on the target. In this work, four combinations of beam energies and targets enabled a rough experimental cross-section to be determined for the first time.

Experimental procedure

The present work consisted of irradiating a neutron-converter thick target with deuterons from the K-130 cyclotron at the JYFL laboratory to produce fast neutrons, and irradiate a target containing water enriched in ^{18}O. The neutron spectra were determined by the activation method applied in our former papers, see *e.g.* ref. [8] and references therein. The production of ^{15}C was obtained via its radioactivity. A 5297.8 keV γ-ray is emitted with a probability of 63.2% per decay (all nuclear data, unless quoted, have been taken from the ENSDF library in NNDC). The 2.45 s half-life of ^{15}C requires a fast transport system to carry the irradiated target to a well-shielded location for counting under lower background than in the cave where it has been irradiated. Such a system had been built for a measurement of production rates of fission products in a uranium target [9]. A schematic layout of the experiment is shown in fig. 1. Here are described the main characteristics of the experiment, in so far they are needed for understanding without going back to our previous papers, and the adaptations made for this work.

Targets and transport system

The targets were water enriched in ^{18}O. The water used in this work was supplied by Campro Scientific [10]. The water had been irradiated by protons to produce ^{18}F and had been recycled. It consequently contained a residual of acetonitrile (CH_3CN) solvant. The respective fractions of oxygen isotopes and solvant were obtained with a gas chromatograph and weighting. The fraction of ^{18}O atoms in the targets was 68(3)%.

The target holder attached to the transport chain was of similar design as the one used in ref. [9], but was bigger and made of aluminum. It had a cavity of 2.5 by 2.5 cm facing the beam and of 3 mm thickness closed with a 1 mm mylar foil. Several water targets of about 2.3 g weight have been used in the course of the experiment. The exact amount of water was obtained by weighting before and after the data had been taken. The cavity could also accomodate metal foils used for measuring the neutron spectrum, squares of 2.5 cm side and 1 mm thickness. The foils were of aluminum, nickel, indium and bismuth. They have been grouped as a stack of Ni, In and Bi foils in the same aluminum holder as it was used for water targets, and as another stack of 3 Al foils in a plastic holder of same geometry. At a given deuteron energy the neutron energy distributions obtained from the analysis of the residual radioactivity of the foils were therefore the same as those which irradiated the water targets. The neutron spectra differed only for the normalisation due to different beam currents and the duration of irradiations. The distance from the 0.5 mm entrance Al window of the neutron-converter target to the center of the 3-foil stack or of the water target was 3.3(1) cm.

The beam current was measured each second using the reading of the charge collected in the neutron-converter target. It allowed numerical integration of the growth and decay equations to be carried out.

The transport system was a loop of a bicycle chain. A single target, either a foil stack or a water target, had been placed in its holder on the chain. The chain was moved by a step motor controlled by a specially-built module. The module sets TTL levels to start and stop the motor, to deflect the ion beam before injection to the cyclotron, and to gate the acquisition. In that way, the beam was off during transport and counting, while counting was enabled only when the target was at its counting position.

Pulsing and gating strongly limits the background due to thermal neutrons having passed the concrete and paraffin shielding. These neutrons (*e.g.* $1.8 \cdot 10^{-10}$ n/cm^2 per deuteron of 40 MeV [9]) activate material near the detector. In ref. [9] radiation induced by thermal neutrons caused a high rejection of true events because they triggerred the active BGO shields surrounding the Ge-clovers. The acceptance, moreover, varied with the time in the cycle. The acquisition needed several seconds to recover its full acceptance. Here, the BGO shields were replaced with a passive lead shield of most often, *i.e.* below and on the sides of the detector cap, 10 cm thickness, and else of 5 cm. The stability of the counting rate of a ^{137}Cs source *versus* time in the counting period showed that the acceptance rate of events did not vary. It was not any longer necessary to make the acquisition in list mode of (time, energy) events, but only to record energy signals as singles.

The activity does not fully fall back to zero after completion of a cycle. It is the so-called build-up. The numerical calculation detailed in ref. [9] has been used here too. The absence of radioactive filiation renders it very simple.

It is interesting to note that a simple analytic formula can be derived in case of constant beam current. The expression for the number of decays N_1 for a single irradiation, *e.g.* for the counting of the foils to measure the neutron spectrum, is well known

$$N_1 = p\,\frac{1-e^{-\lambda t_i}}{\lambda}\,e^{-\lambda t_t}\,(1-e^{-\lambda t_c})$$

with p the production rate (per deuteron in our convention). Indices refer to irradiation (i), transport or waiting (t) and counting (c) times. We derive the overlap for the k-th reaction $\langle\sigma_k\,n\rangle$ via division by the number of atoms per unit surface n_{at}.

$$\langle\sigma_k\,n\rangle = \int \sigma_k(E)\,n(E)\,\mathrm{d}E = p_k/n_{at}.$$

For identical cycles, times and beam current, build-up is governed by a unique parameter $a = e^{-\lambda\,t_{cyc}}$, the cycle time t_{cyc} being $t_i + 2\,t_t + t_c$, while λ is the radioactive constant. The number of decays N_{n_c} cumulated during n_c cycles can be expressed as

$$N_{n_c} = N_1\,n_c\left\{\frac{1}{1-a}\left(1-\frac{a}{n_c}\,\frac{1-a^{n_c}}{1-a}\right)\right\},$$

which gives the expected value of 1 for $a = 0$ and $(n_c{+}1)/2$ in the limit of $a \to 1$ to the correction factor within the braces.

Acquisition and data correction

The γ-rays have been counted by a Ge-detector monocrystal belonging to the phase 1 of the JUROGAM array at JYFL. The counting distance from the detector cap to the center of the 3 mm thick stack or target was 10.2 cm. Corrections for position of the foils in the stack, volume and absorption of the γ-rays have been carried out in the same way as described in our former measurements (ref. [8] and references therein).

The energy spectra have been recorded as gated singles with a Canberra Multi-Channel-Analyser running the Canberra Genie 2000 software. A CAEN two-parameter system [11] has also been used. This system directly analyses the pulses from the preamplifier into histograms. It accepts higher input rates and provides better energy resolution than the conventional analogue acquisition chain. Unfortunately, failure to analyse all high-amplitude pulses such as those of the radioactivity of ^{15}C prevented its use for the quantitative analysis. The system has been yet very useful. Matrices of γ-ray energy *versus* time in cycle helped greatly to sort background γ-rays on the basis of the evolution of their counting rate during the cycle.

It had been noticed during previous experiments that the dead time given by the MCA is underestimated. A calibration was made by looking at the rate of the ^{40}K background peak in the presence of a 1 MBq ^{60}Co source moved from 2.3 m to 10 cm. It covered a range of input rates up to 13 kHz, for which the MCA showed 20% while 27% had been measured. A quadratic correction is suitable in this range. At higher rate the acquisition eventually shows a decreasing dead time, whereas it is actually blocked.

Coincidence-summing corrections have been either calculated in simple cases or have been obtained empirically by recording efficiency curves at various source-to-detector distances. At large distance, *e.g.* 40 cm, the small dispersion of experimental points with respect to the fit verifies that the analysis of peaks is correct. At 10 cm the dispersion increases as the result of the different individual different probabilities for coincidence summing. The effect was significative only for ^{206}Bi decay. The decay scheme is very complex, but two lines are little affected by coincidence summing and can be used as reference. They indicate the actual efficiency for a point source after the usual corrections for the finite size of the foil have been applied back. The 895.1 and 1018.6 keV lines are only in prompt coincidence with the 184.0 keV γ-ray which, moreover, is strongly converted (the total internal conversion coefficient is $\alpha = 1.67$) and attenuated by self-absorption in the Bi-foil and when it passes the In and Ni layers. Indeed, the analytic approximation for γ-rays normal to the foil planes, valid in the large-distance limit, is a transmission of 0.375 of the 184 keV photons. In contrast, the strongest ^{206}Bi lines used for the analysis of neutron spectra, namely the 343.5, 537.5, 803.1, 881.0 and 1718.7 keV, belong to high-multiplicity cascades. Their apparent efficiency was depressed by about 4%, which, according to this discussion, indicates the correction.

Efficiency of the Ge detector at 5 MeV

Derivation of the production rate p of a γ-ray from the peak area implies the knowledge of its decay branching b_γ and of the detector efficiency $\varepsilon(E_\gamma)$. For all lines used in this work, the former are reported with enough accuracy to have negligible impact into the final error. Yet, establishing the Ge-efficiency at 5298 keV, far above the energies of commonly available standards, deserves attention. The efficiency curve up to 1408 keV was made with ^{152}Eu and ^{137}Cs standards (3% error). Some of the activated foils allowed for extra points if their lines are distributed partly inside the calibrated range and partly above. Especially useful is $^{27}\mathrm{Al}(\mathrm{n},\alpha)^{24}\mathrm{Mg}$ offering γ-rays of 1368.6 and 2754.0 keV. A linear function of $\log(\varepsilon)$ *versus* $\log(E_\gamma)$ was used to describe the range from 336 keV —the lowest energy of interest, associated with $^{115}\mathrm{In}(\mathrm{n},\mathrm{n}')^{115}\mathrm{In}^m$— up to 2754 keV. The relative r.m.s. deviation of the points for ^{152}Eu and for foils once the correction for their finite size had been applied was 4% with respect to the fitted curve. All in all, this results in a 5% systematical relative error for the efficiency of the lines used to determine the neutron spectra.

A method to get beyond 2.7 MeV is to use the prompt γ-rays in the thermal-neutron capture by materials close to the detector. Relative intensities per target nucleus are listed in the CapGam library of NNDC. Not only full-energy peaks, but also escape peaks could be exploited. It turned out that the intensity ratios of escape to full-energy peaks do not obviously depend on the direction of the incoming γ-ray. These ratios have been calibrated as a function of γ-ray energy using the 2754 keV line, together with the prompt lines in thermal-neutron captures in the paraffin shielding (^{1}H) and in other materials near the detector. Ten nA of continuous deuteron beam during typically 4 hours turned out to be sufficient to see many strong lines up to 8 MeV. Among the activities with γ-rays of energies below and above 2.7 MeV, the most intense were due to captures by ^{56}Fe (supports, chain), ^{28}Si (concrete) and ^{35}Cl. The first two were by far the strongest. This is due to a large number of atoms rather than a high capture cross-section ($\sigma = 2.59$ b for ^{56}Fe, 0.17 b for ^{28}Si). The spatial distribution of these nuclei is not enough well defined to apply corrections back to a point source. In contrast, ^{35}Cl which presumably is due to spots of cleaning liquid dried on the detector cap has a larger capture cross-section (43.6 b). A measurement with 130 g of NaCl placed at the target position allowed for a source with controlled geometry. After subtracting the background, applying the absorption corrections and a normalisation, the low-energy data points for ε (^{35}Cl) merged with the efficiency curve. The extra points above 2.7 MeV, the most important one at 6111.0 keV, provided references close to the energies of interest. The clearly too low efficiency obtained at 7790.5 keV (^{56}Fe) indicated that the MCA system missed the highest-amplitude pulses too, though only at higher energy and in a smaller fraction than the CAEN system. A quadratic term in $\log(\varepsilon) - \log(E_\gamma)$ starting to act at 2.7 MeV has been added to the linear term to reproduce the efficiency in the high-energy range. Consequently, the extra error increases like $\log^2(E_\gamma/2754)$. The accuracy of the ratio $\varepsilon(5298)/\varepsilon(2754)$ is estimated to 12%. The large error is due to statistics because the added salt did increase the level of ^{35}Cl activity only by 22% of its level in the background.

Measurement procedures

The deuteron beam energies used were 22, 31.5, 40 and 45 MeV. These values result from the request for a short break to change the beam energy. The neutron-converter targets had been planned to be graphite powder all, but D_2O has been used at 22 and 40 MeV. The change of converter target was meant to lower the energy distribution of the neutrons as a substitute for lower beam energy. It had been seen in ref. [5] that the average neutron energy is lower with D_2O or even H_2O than with carbon. The beam current has been adjusted between 10 nA to 100 nA, according to the beam energy, to keep the dead time of the acquisition below 10%.

For neutron measurements a single irradiation of typically half-an-hour, has been carried out for each of the Ni-In-Bi and Al stacks. To account for the very different half-lives of the residual activities, the counting was divided into 3 periods. The first one followed the irradiation for about 2 hours, and was split into short countings for safety. The second one, of 2 to 4 hours, took place when a new beam energy was being prepared, *i.e.* about 20 hours after irradiation. Finally, the third one was done during a few days after the run to obtain better data about the surviving 6.24 days ^{206}Bi and 70.9 days ^{58}Co activities.

The number of cycles for measurements of ^{15}C was about $n = 1000$. The acquisition was divided in at least 3 parts to allow for a check of consistency. A cycle consisted of an irradiation of 6 s, a counting of 12 s, and transport times back and forth of 2 s each. These values have been chosen to avoid large build-up. Typical values for the terms between braces in the build-up formula, were 1.002 (^{15}C) and 1.133 (^{16}N). The 7.13 s ^{16}N activity is produced by (n, p) on ^{16}O remaining in the target.

Table 1. Neutron overlaps in mb for 100 deuterons. The header line shows the deuteron beam energy in MeV and the neutron-converter target. Errors do not include a common scale error of 6%, see text.

Reaction	22, D_2O	31.5, C	40, D_2O	45, C
In(n, n′)	19.0(17)	29.3(16)	59.6(21)	29.4(19)
Ni(n, p)	40.3(19)	67.5(33)	119.4(57)	86.8(45)
Al(n, p)	3.0(14)	7.2(9)	15.0(12)	10.0(8)
Al(n, α)	2.1(2)	6.4(3)	14.1(8)	11.8(6)
Ni(n, 2n)	0.5(1)	2.2(2)	7.5(5)	6.0(3)
Bi(n, 4n)	–	1.0(1)	13.0(6)	12.8(5)

Results

Neutron spectra

Overlaps of cross-section and neutron spectra for reactions with activation foils are shown in table 1. It is remarkable that overlaps at $E_d = 40$ MeV with heavy-water converter are larger than those at 45 MeV with graphite converter. The gain in neutron flux when using D_2O instead of carbon is higher than the increase due to higher beam energy, which empirically [8] is $(45/40)^{2.5} = 1.34$. This confirms the observation that at $E_d = 42$ MeV [5] the neutron flux with heavy-water was 1.5 times higher than with graphite. The table does not include the errors due to the Ge-efficiency, nor another 3% error for the calibration of the beam-current reading device. These errors add 6% to the error on the listed overlaps. Since the reference cross-sections are often given with 10% overall accuracy, addition of all errors suggests that the neutron flux is correct within 15%.

The unfolded experimental neutron spectra are shown in fig. 2. The energy distributions for graphite (solid lines) and heavy water (dashed lines) are clearly different, in agreement with measurements at 40 MeV [9].

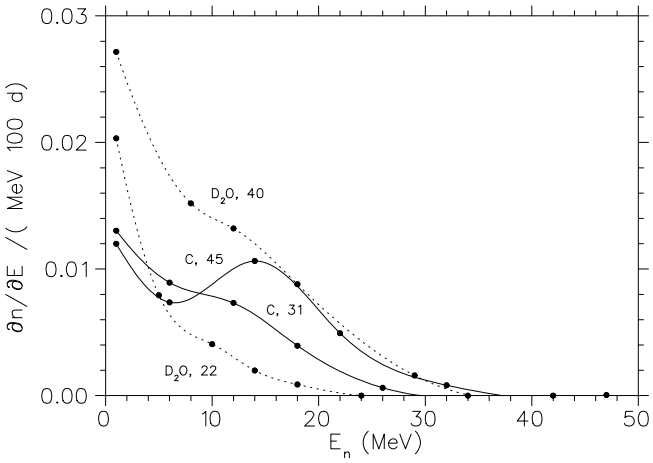

Fig. 2. The neutron spectra seen by the water targets for various deuteron-beam energies and neutron converters. The curves are interpolated between the dots which are the parameters used in the iterative unfolding.

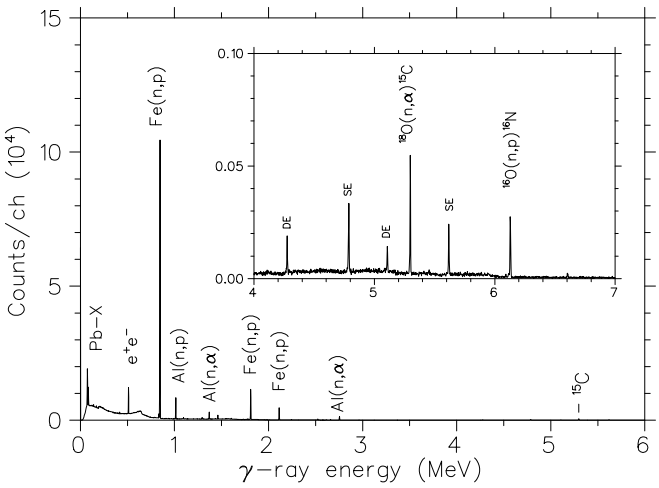

Fig. 3. Gamma spectrum of the water target irradiated by neutrons of d + C at $E_d = 31.5\,\mathrm{MeV}$. The inset (in units of 10^4) shows the γ-rays of interest in this work. The data, taken with 8 nA during 2 hours, represent about 1/3 of the statistics obtained at this beam energy.

The neutron spectra to be expected have been obtained from the interpolation and integration of the double-differential distributions measured previously by us with the same method (ref. [8] and references therein) and of spectra integrated on quite the same angles as this experiment at $E_d = 55\,\mathrm{MeV}$ [12]. At short distance the neutron source cannot be regarded as a point, but is a line corresponding to the range of the deuterons. An estimated center of gravity of neutron emission [12] has been used to define the maximum angle of integration.

It is noteworthy that the integrated flux is on the average 3.4 times less than it has been expected. The result of a misalignment of beam axis and foil has been investigated by integration of the experimental double-differential distributions available from our former experiments, and also by a Monte-Carlo simulation. The calculation was carried out with the Particle and Heavy Ion Transport code Systems (PHITS-3.02) developed at the Japan Atomic Energy Agency [13]. The misalignment is expressed by the angle θ which locates the center of the foil with respect to the nominal beam axis, when it is viewed from the center of the converter. For the 40 MeV deuteron beam on the carbon converter target a decrease by a factor of 3 was obtained for a misalignment of about 25° (experiment) and 30° (simulation) degrees. These values are very surprisingly large. Yet, whatever had happened, the measurements of activation foils and of oxygen targets have been carried out under the same conditions. The experimental neutron spectra must be the ones to use to unfold the overlaps for ^{15}C.

Verification via the ^{16}O(n, p)^{16}N overlaps

Figure 3 shows, as an example, a spectrum of the radioactivity of water target taken at $E_d = 31.5\,\mathrm{MeV}$. The activity is strongly dominated by the ^{56}Fe(n, p)^{56}Mn reaction (threshold = 3.0 MeV) that occurs in the irradiation cave. Part of the chain near the target is activated and is not enough shielded during counting. The 2.58 h half-life of ^{56}Mn is why the dead time does not vary during a cycle. Beam pulsing removes almost all the lines due to thermal-neutron capture, as shown in the inset where only the peaks at 5298 keV (^{15}C) and 6128 keV (^{16}N) and their single (SE) and double (DE) escape peaks emerge above the background.

The cross-section of ^{16}O(n, p)^{16}N is well known up to 20 MeV according to the compilation in NNDC. Evaluations shown in the ENDF library and experimental values shown in the EXFOR library agree. Only one evaluation, namely EAF-2010, and a set of experimental points [14] list values above 30 MeV. The evaluation seems to drop too quickly, whereas the original experimental data points do not connect well neither with the experimental values from other authors nor with the evaluations. We kept the energy dependance of the experimental high-energy tail but connected them to the values below 30 MeV by using a multiplication factor. The uncertainty on the tail of $\sigma(^{16}\mathrm{O(n,p)}^{16}\mathrm{N})$ has no visible impact on the overlaps owing to the small fraction of neutrons contributing to the $\langle \sigma\, n \rangle$ overlaps. The cross-sections for ^{16}O(n, p)^{16}N are shown in fig. 4.

Table 2 shows the experimental overlaps and their ratio to those calculated by folding the experimental neutron spectra shown in fig. 2 with the cross-sections discussed above, fig. 4. The errors quoted are due to counting only. They are mainly due to the dispersion of the results for the various subsets rather than to statistical fluctuations. The unweighted average of the tabulated ratios is 1.10. If one recalls the 13% uncertainty on the Ge-efficiency at 6128 keV and a 10% error on the abundance of ^{16}O in the target, the agreement should appear as an accident. Yet, it tends to show that no large systematical error was bound with the analysis. We note that, if the expected neutron flux had been used instead of the observed one,

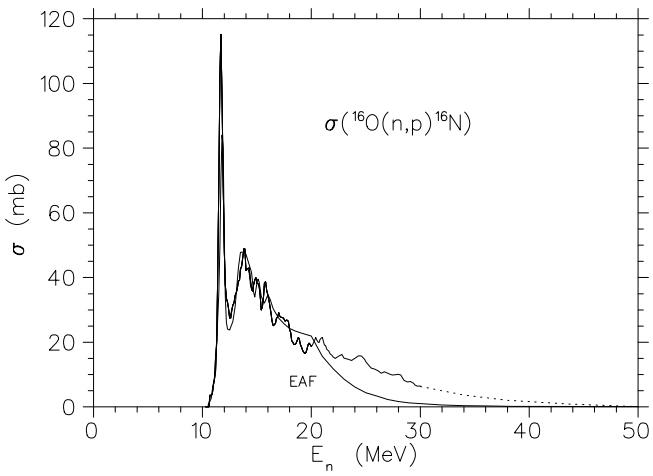

Fig. 4. Cross-sections for ^{16}O(n, p)^{16}N. Below 20 MeV all libraries are in agreement, while above EAF (solid line) decreases faster than the others. The dashed line is an extrapolation that keeps the energy dependence of a measurement, but has been scaled upwards to connect to the bulk of the data.

Table 2. Experimental overlaps (Exper.) in mb for 100 deuterons for ^{16}O(n, p)^{16}N and their ratio to overlaps calculated by folding the experimental neutron spectrum with various cross-sections listed in NNDC; ENDF/B-VII.1, EAF-2010, JEFF-3.2, TENDL16 and RUSFOND-2010. JEFF and TENDL give the same result and are listed together as J,T. A common systematical experimental uncertainty of 17% is not included.

E_d (MeV)	Target	Exper.	ENDF	EAF	J,T	RUSF
22	D_2O	0.55(12)	0.91	0.99	0.91	0.91
31	C	1.65(12)	0.85	0.92	0.85	0.87
40	D_2O	3.46(43)	0.87	0.96	0.87	0.90
45	C	4.71(24)	1.36	1.48	1.36	1.40

three times higher values of expected overlaps had been obtained, in clear discrepancy with the experimental ones. The ratios, however, are not constant. They are slightly lower than 1.0 at $E_d = 22$, 31 and 40 MeV, but the ratio is clearly higher at 45 MeV. The factor 1.4 cannot be accounted for by a realistic increase of the high-energy tail of σ. It is, consequently, probable that there exists some uncontrolled experimental factor. While it had been tempting to readjust the scale to the ^{16}O(n, p)^{16}N data, this procedure is difficult to justify, considering that the experimental uncertainties are larger than the correction factor.

Cross-section of ^{18}O(n, α)^{15}C

Table 3 shows the experimental overlaps and their ratio to calculated overlaps for ^{18}O(n, α)^{15}C. The common systematical error is 14%. The slight decrease with respect to ^{16}O(n, p) results from the smaller relative error on the abundance of ^{18}O. The proposed evaluations in the ENDF NNDC library are now quite different. Only JEFF-3.2 and

Table 3. Experimental overlaps (Exper.) in mb for 100 deuterons for ^{18}O(n, α)^{15}C and their ratio to overlaps calculated by folding the experimental neutron spectrum with various cross-sections listed in NNDC. The libraries do not agree neither with the experiment, nor with each other, except JEFF and TENDL15 listed as J,T showing minor differences. A common systematical experimental error of 14% is not included.

E_d (MeV)	Target	Exper.	EAF	J,T	RUSF
22	D_2O	0.75(12)	4.45	0.42	1.51
31	C	1.60(14)	3.46	0.36–0.38	1.09
40	D_2O	2.04(34)	2.23	0.24	0.63
45	C	1.98(18)	2.67	0.39–0.31	0.74

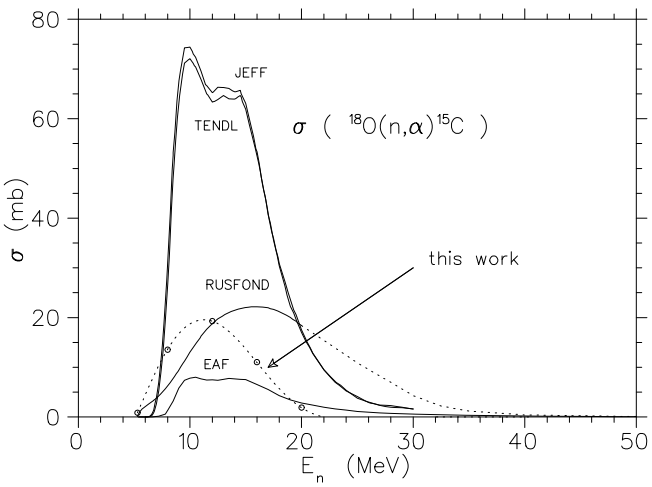

Fig. 5. Cross-sections for ^{18}O(n, α)^{15}C according to libraries evaluated in NNDC (solid lines with labels) and the tentative cross-section extracted in this work by unfolding the overlaps at 4 deuteron beam energies (line with dots). The dashed line of RUSFOND is a tentative extrapolation needed to calculate the overlaps over the whole energy range. Dots do not represent fitted parameters, but are merely a guide to draw the curve by interpolation, see text for more.

ENDF/B-VII are in agreement, but they strongly overestimate the $\langle \sigma\, n \rangle$ overlaps. The other sets EAF-2010, the lowest one, and RUSFOND-2010 underestimate them. Here also, the high-energy tail of cross-sections have been tentatively extrapolated, except for EAF-2010 for which values are listed. The variation of experimental/calculated overlap ratios is an overall decrease with beam energy.

The existence of a set of different neutron spectra could have allowed for an unfolding of the $\langle \sigma\, n_k \rangle$ overlaps in order to extract the cross-section. The method had been similar to the one carried out when the neutron spectra have been obtained, except that the role of spectrum $n_k(E)$ and $\sigma(E)$ had been exchanged. However, the present number of 4 beam energies is too limited for a conventional fit. The cross-section in fig. 5 has therefore been drawn by trial-and-error, moving the dots by steps. During the iterations, the χ^2 of the comparison of experimental and calculated overlaps was kept low, while the curve was constrained by the reaction threshold and the attempt to draw the rising

Table 4. In-target production rates of ^{15}C expected per second for 1 mA of 40 MeV deuterons and other conditions like in this work, but with an expected three times higher flux per deuteron, see text. They are the experimental points (Exper) and points calculated from the fold of neutron spectra, fig. 2, with the tentative cross-section, fig. 5 (Curve). A global systematical error of 14% is not included. The flux (n/s) and median energy E_{med} of the neutrons above 1 MeV are given for quick reference.

E_d (MeV)	Target	Exper.	Curve	n/s (10^{13})	E_{med} (MeV)
		^{15}C/s (10^9)			
22	D_2O	0.97(15)	0.84	1.9	4.7
31	C	2.06(18)	1.84	2.9	8.8
40	D_2O	2.63(43)	3.49	6.1	9.4
45	C	2.55(23)	2.48	3.9	12.9

edge to remind the one of the evaluated cross-sections. The curve presented in fig. 5 is therefore a rough and subjective guess of σ.

Production rate of ^{15}C

The data allow for an estimate of the production rate of ^{15}C in the target of RIB facility, under the same conditions as this experiment. In table 4 the beam intensity has been raised to 1 mA according to the expected performance of the SPIRAL2 linac. The values have been normalised to a weight of 2 g, somewhat less than the various experimental ones, to allow for easier interpolation *versus* beam energy. The abundancy of ^{18}O in the target has been kept to 68%. In addition, the production rates have been scaled up a factor of 3 for the assumed missing neutron flux. The 3% error on the ion-beam current, the 13% due to efficiency of the detector at 5.3 MeV and the 4% on the abundance of ^{18}O in the target, in total a 14% systematical error, should be added to the listed errors. Comparison of the production rates in the columns "exper" and "curve" (calculated by folding) indicates the quality of the adjustment of the proposed $\sigma(E)$ for ^{18}O(n, α)^{15}C.

The thickness used in table 4 is still 3 mm. A longer target, of a few cm, should not be technically problematic, but the increase might be then less than linear with thickness. The geometry varies because of the longer average distance. It is a minor drawback. Another factor is neutron moderation in hydrogen. It may move some neutrons below the peak of sigma and even below the reaction threshold. Yet, in a target of few cm length, a gain factor of 10 may not be unrealistic, so that the production rate of ^{15}C nuclei in the target could reach $2 \cdot 10^{10}$ per second.

Summary and outlook

Summary of the method

Fast neutrons have been produced by stopping deuteron beams in a thick target, the so-called converter. The production of ^{15}C via ^{18}O(n, α)^{15}C, using an enriched water target placed behind the converter, has been studied. In addition, a set of targets chosen for their known neutron-activation cross-sections, $\sigma_k(E)$, have been irradiated in the same geometric conditions. The neutron spectrum $n(E)$ was obtained by unfolding the set of experimental overlaps $\langle \sigma_k\, n \rangle$. Measurements have been repeated at various beam energies in order to obtain different neutron spectra. A tentative unfolding, now with a known neutron spectrum at each beam energy, allowed for a rough estimate of the ^{18}O(n, α)^{15}C cross-section. In the measurement of the production rate all factors need to be known because it is an absolute value. In contrast, the cross-section measurement involves factors, *e.g.* ion-beam current calibration and the scale of the neutron spectra, which cancel. Those which do not, such as target enrichment and weight, acquisition dead time, nuclear decay data, contributed only weakly to the error. All together, 10% accuracy on the cross-section could have been easily reached if the ratio of Ge-efficiencies at 5 MeV and at, say, 1 MeV had been better known. Statistical errors have not been playing a big part in the present measurement neither, being smaller than systematical errors. Based on the counting statistics obtained in this measurement, the lower limit of sensitivity of such a measurement could be for a cross-section peaking at about 1 mb.

The presence of ^{16}N lines in the γ-spectra suggests a comparative measurement as an alternative, if a reference σ is well known. Yet, the energy distribution of the neutrons has to be established at each beam energy. In order to ensure fully identical conditions, the target stack should have included foils for neutron spectra and targets for the σ of interest to be irradiated together.

Scheme for production of ^{15}C

The production rate of ^{15}C to be expected in the target at SPIRAL2 is estimated from this experiment by scaling the data. With 1 mA of 40 MeV deuterons on a carbon converter, a water target of 6 cm^2 area and 4 cm length with 70% enrichment in ^{18}O, the ^{15}C rate is a few 10^{10} per second.

The proposed target construction is a cell filled with water enriched in ^{18}O, with perhaps a supply of oxygen to saturate the liquid, and a tube to extract CO_2. The cell can be placed behind the neutron converter, quite near and is at room temperature. It is a very safe construction. Release of ^{15}C combined with oxygen as bubbles should be fast and efficient, in contrast to the options with a heated solid target. The loss factors are therefore those during ionisation, maybe optional charge breeding, and acceleration. They cannot be avoided in the ISOL method and deserve a further independent study.

The authors acknowledge the support of several groups at Jyväskylä for lending various equipments: IGISOL (now Exotic Nuclei and Beams) for the Multi-Channel Analyser, RITU-GAMMA (now Nuclear Spectroscopy) for the Ge-detector and the CAEN acquisition module, and the RADEF group for the

beam current monitoring module. They are also indebted in Mr. J. Hyvönen who kindly accepted to change the beam energy outside of his regular schedule. One author (GL) wishes to thank both the GANIL and JYFL laboratories for granting e-mail and computer access.

Data Availability Statement This manuscript has no associated data or the data will not be deposited. [Authors' comment: All relevant data are in the tables.]

Publisher's Note The EPJ Publishers remain neutral with regard to jurisdictional claims in published maps and institutional affiliations.

Open Access This is an open access article distributed under the terms of the Creative Commons Attribution License (http://creativecommons.org/licenses/by/4.0), which permits unrestricted use, distribution, and reproduction in any medium, provided the original work is properly cited.

References

1. M.G. Saint-Laurent, G. Lhersonneau, J. Aystö, S. Brandenburg, A.C. Mueller, J. Vervier, *SPIRAL Phase II European RTT Final Report*, in2p3-00263539 (2001) `http://hal.in2p3.fr/in2p3-00263539`.
2. S. Galès, Nucl. Phys. A **834**, 717 (2010) and `http://www.ganil-spiral2.eu/`.
3. X. Ledoux, M. Aïche, M. Avrigeanu, V. Avrigeanu, E. Balanzat *et al.*, Radiat. Prot. Dosim. **180**, 115 (2018) and hal-01669642, `https://hal.archives-ouvertes.fr/hal-01669642`.
4. A. Pichard, PhD Thesis, *Développement de faisceaux d'ions radioactifs pour le projet SPIRAL 2*, Université de Caen (2010) and `https://tel.archives-ouvertes.fr/tel-00544206`.
5. G. Lhersonneau, T. Malkiewicz, K. Kolos, M. Fadil, H. Kettunen, M.G. Saint-Laurent, A. Pichard, W.H. Trzaska, G. Tyurin, L. Cousin, Nucl. Instrum. Methods Phys. Res. A **603**, 228 (2009).
6. M. Berridge, R. Kjellstrm, Appl. Radiat. Isot. **50**, 699 (1999).
7. National Nuclear Data Center, *Evaluated (ENDF) and experimental (EXFOR) cross-sections, reaction Q-values, evaluated decay and structure data (ENSDF), and thermal-neutron capture γ-rays (CapGam)*, `https://www.nndc.bnl.gov`.
8. G. Lhersonneau, T. Malkiewicz, M. Fadil, D. Gorelov, P. Jones, P.Z. Ngcobo, J. Sorri, W.H. Trzaska, Eur. Phys. J. A **52**, 364 (2016).
9. G. Lhersonneau, T. Malkiewicz, P. Jones, P. Karvonen, S. Ketelhut, O. Bajeat, M. Fadil, S. Gaudu, M.G. Saint-Laurent, W.H. Trzaska, Nucl. Instrum. Methods Phys. Res. A **698**, 224 (2013).
10. Campro Scientific GmbH, Berlin, Germany, `www.campro.eu/`.
11. Dual Digital Multi Channel Analyzer DT5780, `https://www.caen.it/products/dt5780/`.
12. G. Lhersonneau, T. Malkiewicz, P. Jones, S. Ketelhut, W.H. Trzaska, Eur. Phys. J. A **48**, 116 (2012).
13. T. Sato, Y. Iwamoto, S. Hashimoto, T. Ogawa, T. Furuta, S. Abe, T. Kai, P.E. Tsai, N. Matsuda, H. Iwase, N. Shigyo, L. Sihver, K. Niita, J. Nucl. Sci. Technol. **55**, 684 (2018).
14. R.O. Nelson, M.B. Chadwick, A. Michaudon, P.G. Young, Nucl. Sci. Eng. **138**, 105 (2011).